Study of Nanoscratching Process of GaAs Using Molecular Dynamics

Defu Yi [1], Jianyong Li [1,2] and Pengzhe Zhu [1,2,*]

[1]   School of Mechanical, Electronic and Control Engineering, Beijing Jiaotong University, Beijing 100044, China; 11116322@bjtu.edu.cn (D.Y.); jyli@bjtu.edu.cn (J.L.)
[2]   Key Laboratory of Vehicle Advanced Manufacturing, Measuring and Control Technology, Ministry of Education, Beijing 100044, China
*   Correspondence: pzzhu@bjtu.edu.cn

Abstract: In this paper, molecular dynamics method was employed to investigate the nanoscratching process of gallium arsenide (GaAs) in order to gain insights into the material deformation and removal mechanisms in chemical mechanical polishing of GaAs. By analyzing the distribution of hydrostatic pressure and coordination number of GaAs atoms, it was found that phase transformation and amorphization were the dominant deformation mechanisms of GaAs in the scratching process. Furthermore, anisotropic effect in nanoscratching of GaAs was observed. The diverse deformation behaviors of GaAs with different crystal orientations were due to differences in the atomic structure of GaAs. The scratching resistance of GaAs(001) surface was the biggest, while the friction coefficient of GaAs(111) surface was the smallest. These findings shed light on the mechanical wear mechanism in chemical mechanical polishing of GaAs.

Keywords: GaAs; molecular dynamics; nanoscratch; anisotropic effect; phase transformation

1. Introduction

Gallium arsenide (GaAs) wafer has applications in numerous fields, such as illumination, photoelectric detection, and solar energy, due to its excellent mechanical and electronic properties. For example, GaAs wafers with a super smooth surface are needed for the production of high-quality flexible solar cells and light emitting diode (LED) [1,2]. At present, chemical mechanical polishing (CMP) is critically required to fabricate GaAs wafer with a super smooth and planar surface. Many researchers have investigated the CMP process of GaAs. For instance, subnanometer surface finish was achieved in CMP of GaAs [3]. Matovu et al. studied the material removal in the CMP process of GaAs with SiO_2 particles [4]. Yu et al. found that high polishing speed using polishing slurry containing SiO_2 particles leads to high material removal rate of GaAs [5]. Due to the complexity of the CMP process, the material removal mechanisms in CMP of GaAs are still not fully understood [6].

Since the CMP process only involves the material deformation and removal of a few atomic layers, continuous mechanics is not fully applicable in the description of the removal process. Molecular dynamics (MD) method—a powerful tool to describe the atomic scale details of various phenomena—has been widely employed to explore the mechanical wear mechanism in the CMP process [7,8]. Ye et al. found that adding chemical effect results in a smooth surface during the polishing of a copper surface using MD [9]. In MD simulations, Han et al. showed that ductile material removal was critical in realizing a super smooth surface of the silicon CMP process [10]. Si et al. proposed the monoatomic layer removal mechanism during CMP of silicon using MD simulations of nanoscratching [11]. To date, few literatures have focused on the CMP process of GaAs using MD, though some scholars have simulated the nanoscratching process of GaAs [12]. The deformation

mechanisms of a workpiece are closely related to the material removal in the CMP process. It has been found that plastic deformation of GaAs results from dislocation motion during the scratching [12,13]. However, phase transformation in crystalline GaAs has also been reported in MD simulations of nanoindentation [14,15], implying different deformation mechanisms.

To further explore the material removal mechanisms in the CMP process of GaAs, we carried out in this paper MD simulations to study the nanoscratching of GaAs. We mainly investigated the material deformation and removal mechanisms in GaAs.

2. Simulation Method

The MD simulation model of scratching process is shown in Figure 1. The model was made up of a GaAs workpiece with zinc blende (ZB) structure and a rigid spherical abrasive. The GaAs workpiece had a size of 42 a × 28 a × 13 a (a = 0.565 nm, the lattice constant of GaAs). The orientations of the workpiece were in x-[100], y-[010] and z-[001]. The workpiece could be divided into three parts—boundary layer, thermostat layer, and Newtonian layer. The bottom (four layers of atoms) of the workpiece was fixed to restrict any translation of the workpiece. The six layers of atoms adjacent to the boundary layer at the bottom of GaAs were the thermostat layer where atoms were kept at 300 K by velocity scaling method to mimic the heat dissipation in scratching process. All the simulations were carried out using LAMMPS [16] with an integration timestep of 1 fs. Periodic boundary conditions were imposed in the x and y directions.
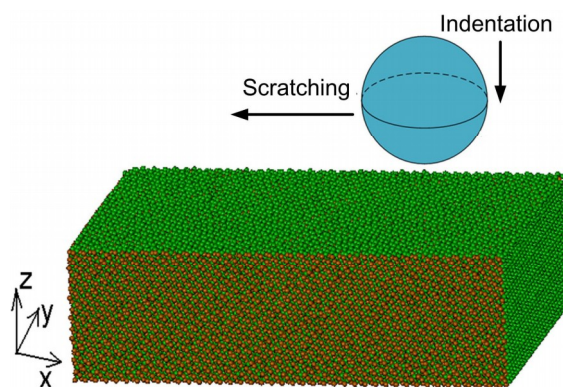
Figure 1. Model of molecular dynamics (MD) simulation. The green atoms and orange atoms are Ga atoms and As atoms, respectively.

The atomic interactions between GaAs workpiece atoms were described by bond-order potentials (BOP) [17,18].

The interaction between the workpiece and abrasive was modeled by a repulsive potential [19,20]. The radius of the abrasive was 4 nm.

In the simulations, we performed scratching along the negative x direction. As the indentation and scratching velocities of most MD simulations are 1~200 m/s [21–27], 100 m/s was adopted for both the indentation and scratching process in this paper. The scratching distance was 10 nm.

3. Results and Discussions

3.1. The Deformation Behaviors of GaAs(001)

The typical deformation behaviors of GaAs(001) in the scratching are shown in Figure 2. The GaAs underwent elastic and plastic deformation in the scratching process. Side flow was formed as some workpiece atoms accumulated on two sides of the abrasive. Chip was formed because some workpiece atoms piled up ahead of the abrasive. In real CMP process, the removed material can be polished away by slurry.
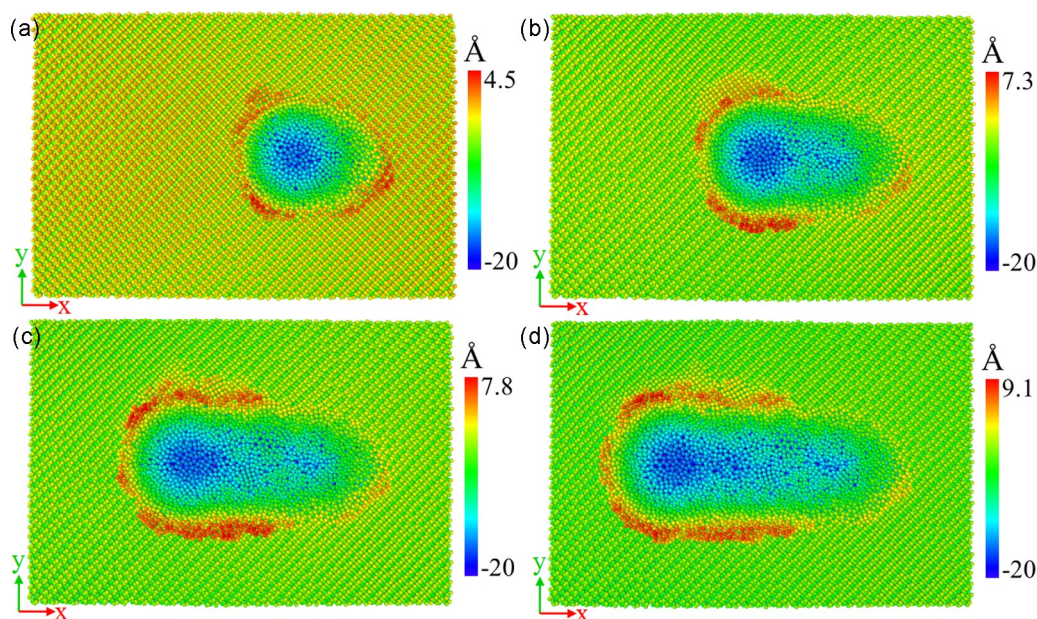
Figure 2. Deformation behaviors of GaAs(001) in scratching at sliding distances of (**a**) 2 nm; (**b**) 5 nm; (**c**) 8 nm; and (**d**) 10 nm. The scratching depth is 1.5 nm. Atoms are colored by heights in z direction.

In the scratching process, no dislocation nucleation and movement were observed and amorphous structure was formed, which implies that phase transformation and amorphization may have occurred. It has been reported that GaAs undergoes a phase transformation from a zinc blende structure to a rocksalt, one at a pressure of about 17 GPa [28] and more recently at a pressure of 12 ± 1.5 GPa [29]. To determine whether GaAs undergoes a phase transformation, the distribution of hydrostatic pressure of the workpiece is required. Therefore, we calculated the atomic stresses using the virial theorem and then averaged the stresses over a 4 Å spherical volume around each atom (see Figure 3). The maximum hydrostatic pressure under the abrasive in the scratching process was about 17 GPa, matching the criterion of phase transformation to a rocksalt structure.
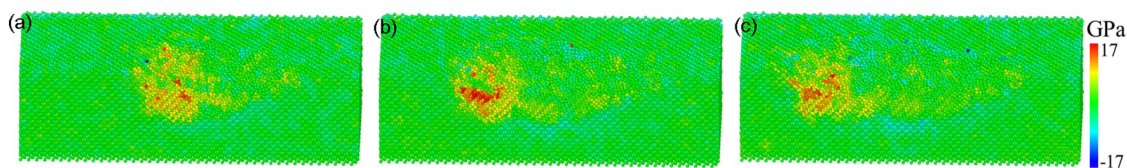

Figure 3. Distribution of hydrostatic pressure under the abrasive ($y > 0$) in various scratching stages in the scratching. The sliding distance is (**a**) 5 nm; (**b**) 8 nm; and (**c**) 10 nm. The scratching depth is 1.5 nm.

The coordination number (CN) is widely used to describe the deformation behaviors of silicon and germanium in the nanoindentation and scratching process [30–32]. MD simulations of the nanoindentation process on silicon and germanium have shown that phase transformation takes place under high pressure [30,31]. It is well known that atoms with CN of 4 indicate a zinc blende structure. Sixfold-coordinated atoms indicate a rocksalt structure. Atoms with CN of 5 could be an intermediate in the formation of a rocksalt structure. Atoms with CN of less than 4 are surface atoms, and atoms with CN of higher than 6 make up the amorphous structure. It can be seen in Figure 4 that a sixfold-coordinated rocksalt structure formed just beneath the abrasive. In the scratching, more and more sixfold-coordinated rocksalt phase were generated in the workpiece due to the pressure induced by the abrasive. In addition, the high stress produced by the abrasive in the scratching also enabled the generation of an amorphous structure in the machining region [33]. Moreover, the number

of amorphous structure atoms increased with the advance of the abrasive. It has been found that direct amorphization is the primary deformation of germanium besides the limited phase transformation due to the high and complex stress states in the cutting/scratching process [33]; this was similar to our simulation results. Our simulations showed that phase transformation and amorphization were the dominant deformation mechanisms of GaAs in the scratching process.
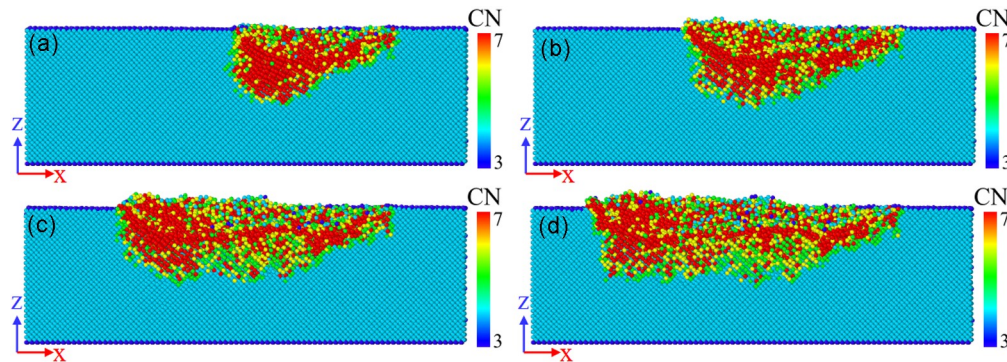

Figure 4. Cross-sectional view of deformation behaviors of GaAs(001) in scratching at sliding distances of (**a**) 2 nm; (**b**) 5 nm; (**c**) 8 nm; and (**d**)10 nm. The scratching depth is 1.5 nm. The atoms are colored by coordination number (CN).

To further study the deformation behavior of GaAs, we recorded the variation of coordination number of workpiece atoms in the scratching (see Figure 5). The scratching depth was 1.5 nm. It was found that with abrasive scratches of the workpiece, the number of fourfold-coordinated atoms decreased, while the number of sixfold-coordinated atoms increased. This is due to the fact that in the scratching process, the high stress produced by the abrasive induces the phase transformation from a zinc blende to a rocksalt structure [15,28,29].
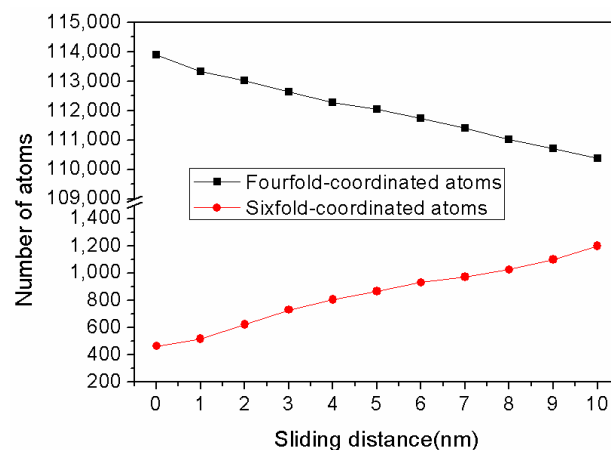

**Figure 5.** Variation of the number of atoms with coordination number in scratching process.

Figure 6 shows the deformation behaviors of GaAs for different scratching depths. With the increase of scratching depth, more workpiece atoms were removed and bigger deformation occurred. The variations of normal force and friction force during scratching process are recorded in Figure 7. It can be seen that after initial stage of scratching, both the normal force and the friction force arrived at a steady state, only fluctuating around certain values. The fluctuation of forces mainly resulted from thermal motion of atoms and phase transformation in the workpiece. The average forces were calculated for the scratching distance from 2 nm to 10 nm (see Figure 8). As expected, a bigger scratching depth led to larger friction force and normal force due to more contacting atoms and larger deformation.
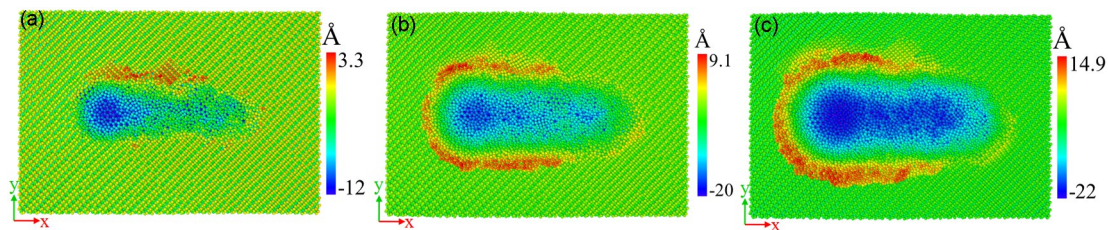
Figure 6. Top views of the GaAs(001) at a scratching distance of 10 nm for different scratching depths of (**a**) 1.0 nm; (**b**) 1.5 nm; and (**c**) 2.0 nm. Atoms are colored by heights in z direction.
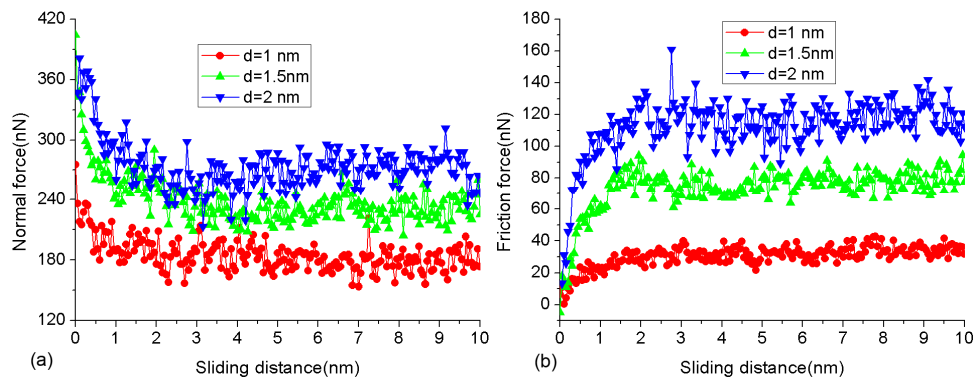
Figure 7. Force-displacement curves in the scratching process for different scratching depths. (**a**) normal force and (**b**) friction force.
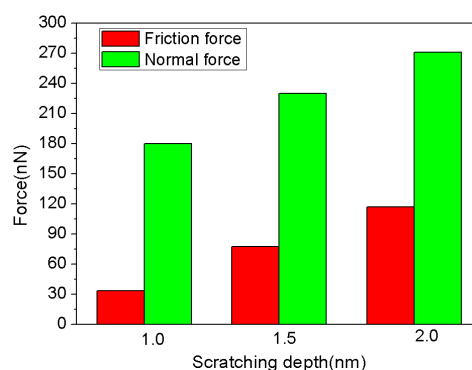

Figure 8. The average normal force and friction force for different scratching depths.

3.2. The Anisotropic Effects

Since single crystalline semiconductor materials exhibit anisotropic effects in nanoindentation and nanoscratch, nanoscratching simulations on GaAs(110) and (111) surfaces were also conducted. For GaAs(110) surface, *x* was along [001], *y* along [110] and *z* along [110]. For GaAs(111) surface, *x* was along [1-10], *y* along [11-2] and *z* along [111]. The scratching direction was along the negative *x* direction. Other simulation details were the same as those in the simulation of the GaAs(001) surface.

The top view and cross-sectional view of deformation behaviors of the GaAs workpiece for different crystal orientations are shown in Figures 5 and 9, respectively. We could see the diverse deformation behaviors of GaAs with different crystal orientations resulting from the different atomic structure of GaAs. The height of pile-up atoms at a sliding distance of 10 nm and scratching depth of 1.5 nm was the biggest for GaAs(001) (9.1 Å) and the smallest for GaAs(110) (6.9 Å). Moreover, it can be seen from Figure 10 that a phase transformation from a zinc blende structure to a rocksalt one had also taken place in the scratching process for GaAs(110) surface and GaAs(111) surface like the GaAs(001)

surface. However, the distribution of subsurface phase transformation zone was different for different crystal orientations of GaAs (see Figures 5 and 10).
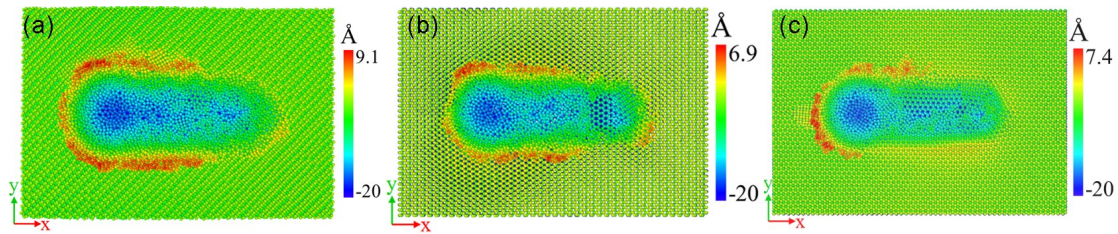

Figure 9. Top view of deformation behaviors of GaAs at a sliding distance of 10 nm for (**a**) GaAs(001); (**b**) GaAs(110); and (**c**) GaAs(111). The scratching depth is 1.5 nm. Atoms are colored by heights in *z* direction.
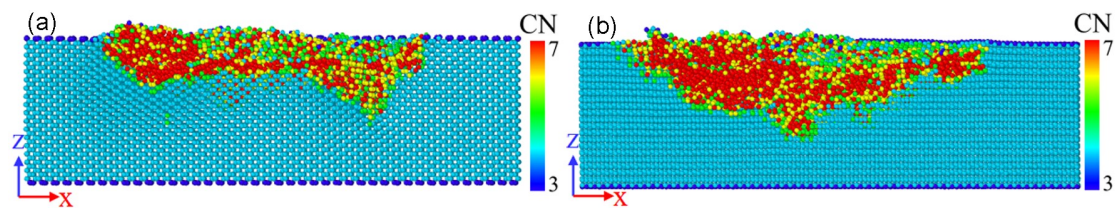
Figure 10. Cross-sectional view of deformation behaviors of (**a**) GaAs(110) and (**b**) GaAs(111) at a sliding distance of 10 nm. The scratching depth is 1.5 nm. The atoms are colored by CN.

Figure 11 shows the average friction force, normal force, and friction coefficient for different crystallographic orientations during the scratching process. It is reasonable that the average friction force and normal force are larger for a bigger scratching depth. As the atomic area density and the interlayer distance were different for different crystal orientations of GaAs, the number of contacting atoms was different for various crystal orientations of GaAs. Therefore, the friction force and normal force could not be employed to measure the scratching resistance. The scratching resistance is usually measured by friction coefficient, defined as the ratio of friction force to normal force. Figure 11c shows the calculated friction coefficients. Table 1 shows the atomic planar density and interplanar spacing with respect to the orientation of GaAs. It should be noted that the two nearest (111) planes of GaAs are usually considered as a single atomic plane called compound (111) plane. It can be seen that the anisotropic effect of the average friction coefficient in the scratching was related to the differences of atomic planar density and interplanar spacing of GaAs. For the GaAs(001) [100] combination, the friction coefficients were the biggest, while both the atomic planar density and interplanar spacing were the smallest. Moreover, the friction coefficients of GaAs(111) [1-10] combination were the smallest and both the atomic planar density and interplanar spacing of compound GaAs(111) were the biggest; the friction coefficients of GaAs(110) [001] combination were in between the two, as were the atomic planar density and interplanar spacing of GaAs(110).
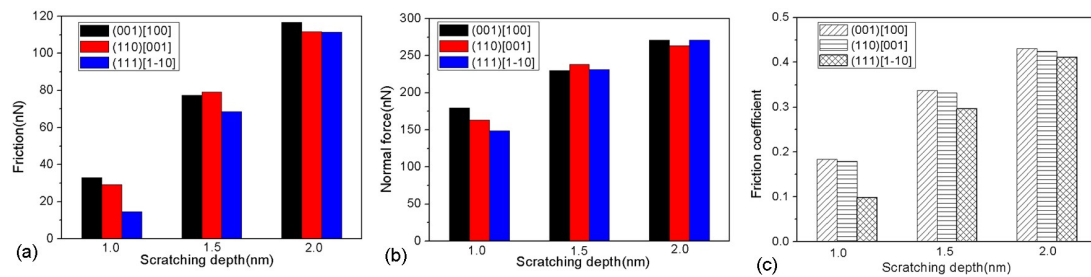
Figure 11. (**a**) The average friction force; (**b**) normal force; and (**c**) friction coefficient in scratching process for different crystallographic orientations.

Table 1. Atomic density and distance between the planes for GaAs.

Orientation	Atomic Density per Unit Area	Distance between Planes
{001}	$\frac{2}{a^2}$	$\frac{a}{4}$
{110}	$\frac{2\sqrt{2}}{a^2}$	$\frac{\sqrt{2}a}{4}$
compound{111}	$\frac{8\sqrt{3}}{3a^2}$	$\frac{\sqrt{3}a}{4}$

a is the lattice constant of GaAs and *a* = 0.565 nm.

4. Conclusions

In this paper, MD simulations were performed to explore the material removal in the CMP process of GaAs. The deformation mechanisms and crystal anisotropic effects in the scratching process were thoroughly investigated. The following conclusions are obtained:

(1) By analyzing the distribution of hydrostatic pressure and coordination number of GaAs atoms, it was found that phase transformation and amorphization were the dominant deformation mechanisms of GaAs in nanoscratching process.

(2) There existed significant anisotropic effect in nanoscratching of GaAs. The different deformation behaviors of GaAs with various crystal orientations were due to the differences in the atomic structure of GaAs. The friction coefficient (scratching resistance) of GaAs(001) [100] combination was the biggest, while the friction coefficient of GaAs(111) [1-10] combination was the smallest; the friction coefficient of GaAs(110) [001] combination was in between the two.

Conflicts of Interest: The authors declare no conflict of interest.

References

1. Wasmer, K.; Parlinska-Wojtan, M.; Graça, S.; Michler, J. Sequence of deformation and cracking behaviours of Gallium-Arsenide during nano-scratching. *Mater. Chem. Phys.* **2013**, *138*, 38–48. [CrossRef]
2. Lastras-Martínez, L.; Castro-García, R.; Balderas-Navarro, R.; Lastras-Martínez, A. Microreflectance difference spectrometer based on a charge coupled device camera: surface distribution of polishing-related linear defect density in GaAs (001). *Appl. Opt.* **2009**, *48*, 5713–5717. [CrossRef] [PubMed]
3. McGhee, L.; McMeekin, S.G.; Nicol, I.; Robertson, M.I.; Winfield, J.M. Chemomechanical polishing of gallium arsenide and cadmium telluride to subnanometre surface finish. Evaluation of the action and effectiveness of hydrogen peroxide, sodium hypochlorite and dibromine as reagents. *J. Mater. Chem.* **1994**, *4*, 29–34. [CrossRef]
4. Matovu, J.; Ong, P.; Leunissen, L.; Krishnan, S.; Babu, S. Fundamental investigation of chemical mechanical polishing of GaAs in silica dispersions: material removal and arsenic trihydride formation pathways. *ECS J. Solid State Sci. Technol.* **2013**, *2*, P432–P439. [CrossRef]

5. Yu, B.; Gao, J.; Chen, L.; Qian, L. Effect of sliding velocity on tribochemical removal of gallium arsenide surface. *Wear* **2015**, *330*, 59–63. [CrossRef]

6. Zhao, D.; Lu, X. Chemical mechanical polishing: theory and experiment. *Friction* **2013**, *1*, 306–326. [CrossRef]

7. Chen, R.; Luo, J.; Guo, D.; Lu, X. Extrusion formation mechanism on silicon surface under the silica cluster impact studied by molecular dynamics simulation. *J. Appl. Phys.* **2008**, *104*, 104907. [CrossRef]

8. Si, L.; Guo, D.; Luo, J.; Lu, X.; Xie, G. Abrasive rolling effects on material removal and surface finish in chemical mechanical polishing analyzed by molecular dynamics simulation. *J. Appl. Phys.* **2011**, *109*, 084335. [CrossRef]

9. Ye, Y.; Biswas, R.; Bastawros, A.; Chandra, A. Simulation of chemical mechanical planarization of copper with molecular dynamics. *Appl. Phys. Lett.* **2002**, *81*, 1875–1877. [CrossRef]

10. Han, X.; Hu, Y.; Yu, S. Investigation of material removal mechanism of silicon wafer in the chemical mechanical polishing process using molecular dynamics simulation method. *Appl. Phys. A* **2009**, *95*, 899–905. [CrossRef]

11. Si, L.; Guo, D.; Luo, J.; Lu, X. Monoatomic layer removal mechanism in chemical mechanical polishing process: A molecular dynamics study. *J. Appl. Phys.* **2010**, *107*, 064310. [CrossRef]

12. Fang, T.-H.; Lin, S.-J.; Hong, Z.-H.; Shen, S.-T.; Huang, C.-T. Mechanical characteristics of nanoscratched gallium arsenide using molecular dynamics simulation. *Nanosci. Nanotechnol. Lett.* **2010**, *2*, 220–225. [CrossRef]

13. Wasmer, K.; Parlinska-Wojtan, M.; Gassilloud, R.; Pouvreau, C.; Tharian, J.; Micher, J. Plastic deformation modes of gallium arsenide in nanoindentation and nanoscratching. *Appl. Phys. Lett.* **2007**, *90*, 031902. [CrossRef]

14. Rino, J.P.; Chatterjee, A.; Ebbsjö, I.; Kalia, R.K.; Nakano, A.; Shimojo, F.; Vashishta, P. Pressure-induced structural transformation in GaAs: A molecular-dynamics study. *Phys. Rev. B* **2002**, *65*, 195206. [CrossRef]

15. Chrobak, D.; Nordlund, K.; Nowak, R. Nondislocation origin of GaAs nanoindentation pop-in event. *Phys. Rev. Lett.* **2007**, *98*, 045502. [CrossRef] [PubMed]

16. Plimpton, S. Fast parallel algorithms for short-range molecular dynamics. *J. Comput. Phys.* **1995**, *117*, 1–19. [CrossRef]

17. Pettifor, D.; Oleinik, I. Analytic bond-order potential for open and close-packed phases. *Phys. Rev. B* **2002**, *65*, 172103. [CrossRef]

18. Murdick, D.; Zhou, X.; Wadley, H.; Nguyen-Manh, D.; Drautz, R.; Pettifor, D. Analytic bond-order potential for the gallium arsenide system. *Phys. Rev. B* **2006**, *73*, 045206. [CrossRef]

19. Kelchner, C.L.; Plimpton, S.; Hamilton, J. Dislocation nucleation and defect structure during surface indentation. *Phys. Rev. B* **1998**, *58*, 11085. [CrossRef]

20. Ziegenhain, G.; Hartmaier, A.; Urbassek, H.M. Pair vs many-body potentials: Influence on elastic and plastic behavior in nanoindentation of fcc metals. *J. Mech. Phys. Solids* **2009**, *57*, 1514–1526. [CrossRef]

21. Zhu, P.-Z.; Hu, Y.-Z.; Ma, T.-B.; Wang, H. Molecular dynamics study on friction due to ploughing and adhesion in nanometric scratching process. *Tribol. Lett.* **2011**, *41*, 41–46. [CrossRef]

22. Mulliah, D.; Kenny, S.; Smith, R.; Sanz-Navarro, C. Molecular dynamic simulations of nanoscratching of silver (100). *Nanotechnology* **2003**, *15*, 243. [CrossRef]

23. Yan, Y.; Sun, T.; Dong, S.; Luo, X.; Liang, Y. Molecular dynamics simulation of processing using AFM pin tool. *Appl. Surf. Sci.* **2006**, *252*, 7523–7531. [CrossRef]

24. Pei, Q.; Lu, C.; Lee, H. Large scale molecular dynamics study of nanometric machining of copper. *Comput. Mater. Sci.* **2007**, *41*, 177–185. [CrossRef]

25. Zhang, J.; Sun, T.; Yan, Y.; Liang, Y. Molecular dynamics study of scratching velocity dependency in AFM-based nanometric scratching process. *Mater. Sci. Eng. A* **2009**, *505*, 65–69. [CrossRef]

26. Zhang, J.; Zhang, J.; Wang, Z.; Hartmaier, A.; Yan, Y.; Sun, T. Interaction between phase transformations and dislocations at incipient plasticity of monocrystalline silicon under nanoindentation. *Comput. Mater. Sci.* **2017**, *131*, 55–61. [CrossRef]

27. Yuan, Y.; Sun, T.; Zhang, J.; Yan, Y. Molecular dynamics study of void effect on nanoimprint of single crystal aluminum. *Appl. Surf. Sci.* **2011**, *257*, 7140–7144. [CrossRef]

28. Weir, S.T.; Vohra, Y.K.; Vanderborgh, C.A.; Ruoff, A.L. Structural phase transitions in GaAs to 108 GPa. *Phys. Rev. B* **1989**, *39*, 1280. [CrossRef]

29. Besson, J.; Itie, J.; Polian, A.; Weill, G.; Mansot, J.; Gonzalez, J. High-pressure phase transition and phase diagram of gallium arsenide. *Phys. Rev. B* **1991**, *44*, 4214. [CrossRef]

30.	Zarudi, I.; Cheong, W.; Zou, J.; Zhang, L. Atomistic structure of monocrystalline silicon in surface nano-modification. *Nanotechnology* **2003**, *15*, 104. [CrossRef]

31.	Zhu, P.; Fang, F. Molecular dynamics simulations of nanoindentation of monocrystalline germanium. *Appl. Phys. A* **2012**, *108*, 415–421. [CrossRef]

32.	Lai, M.; Zhang, X.; Fang, F.; Wang, Y.; Feng, M.; Tian, W. Study on nanometric cutting of germanium by molecular dynamics simulation. *Nanoscale Res. Lett.* **2013**, *8*, 13. [CrossRef] [PubMed]

33.	Lai, M.; Zhang, X.; Fang, F. Crystal orientation effect on the subsurface deformation of monocrystalline germanium in nanometric cutting. *Nanoscale Res. Lett.* **2017**, *12*, 296. [CrossRef] [PubMed]